

# Microscopic thermal machines using run-and-tumble particles

Aradhana Kumari\* and Sourabh Lahiri†

Department of Physics, Birla Institute of Technology Mesra, Ranchi, Jharkhand 835215

## Abstract

Microscopic thermal machines that are of the dimensions of around few hundred nanometers have been the subject of intense study over the last two decades. Recently, it has been shown that the efficiency of such thermal engines can be enhanced by using active Brownian particles. In this work, we numerically study the behaviour of tiny engines and refrigerators that use an active run-and-tumble particle. We find that the results for the engine mode are in sharp contrast with those of engines using active Brownian particles. The efficiency of an engine using a run-and-tumble particle is found to be smaller in general than a passive microscopic engine. However, when the applied protocol is time-reversed, the resulting microscopic refrigerator can have a much higher coefficient of performance under these conditions. The engine as well as refrigerator are shown to have enhanced performance when the mass of the particle becomes smaller.

## 1 Introduction

Microscopic heat engines and refrigerators have been in the focus for the last two decades due to their possible applications across various fields. Micro-engines can find potential uses in the field of nanomachines and nanobots, which in turn would find applications in many areas, especially in medicine [1]. An efficient microscopic engine needs to be developed in order to power such small machines. Several models have been proposed in the literature and have been realized experimentally, that would act as tiny heat engines [2–7]. A nice review on microscopic heat engines has been provided in [8]. The extension to quantum dynamics has been done [9, 10].

It was shown in [3, 4] that an engine using an active Brownian particle (ABP) trapped in a harmonic potential as its working system turns out to be more efficient than its passive counterpart. The activity was introduced by means of an exponentially correlated noise that introduced finite persistence in the motion of the particle. If such engines are driven in a time-reversed manner, then they can also lead to microscopic refrigerators [11, 12]. Such refrigerators have also been modelled by using a sawtooth potential in presence of an external drive and have been studied in [13–15]. Refrigeration in presence of velocity-dependent feedback control has been studied in [16–18]. In [16], the authors demonstrated how the accuracy of an AFM cantilever can be enhanced by reducing its thermal noise. Another potential application is in intramolecular cooling which, if achieved, can be beneficial in selecting certain reaction channels over others or for increasing the efficiency of catalysis [19]. Study of self-contained microscopic heat engines and refrigerators have been done for quantum systems [20, 21].

We use an active run-and-tumble particle as the working system of the engine and the refrigerator, unlike the active Brownian particle used in [4]. Run-and-tumble (RT) particles

---

\*Email: aradhanakumari2546@gmail.com

†Email: sourabhlahiri@gmail.com

provide an alternative model for activity, which is considered to be a more realistic model for describing motion of flagellar cells like the E. Coli in a stimulus-free environment [22]. They swim forward while their flagella spin counter-clockwise. However, once the direction of spin becomes clockwise, the flagella unbundle and the cell undergoes a rotation about its centre of mass. In [23–25], the authors have provided Langevin equations that capture the statistics of such motion. An effective Smoluchowski equation for RT motion in presence of taxis effects was developed in [26]. The RT motion in one-dimension under confinements has been modelled by a Langevin equation involving a telegraphic noise in [27]. The dynamics has been contrasted with that of the ABPs in [28]. For a recent review on the physics of such microswimmers, see [29]. Recently, it has been shown that RT particles can be prepared artificially by using synthetic Janus particles subjected to an electric field [30].

We explore the behaviour of the RT particle in order to study its effects on the efficiency of thermal engines and refrigerators. At first we show that the results of our simulations are in agreement with the analytical results of [23, 31]. Then we use simulations to study the system under the more general conditions where the stiffness parameter of the trapping potential changes periodically with time. In addition to the usual RT motion, the particle is subjected to thermal noise due the presence of the two heat baths at different temperatures that are required for the working of the engine/refrigerator. We closely follow the approach of [23] in modelling our dynamics for an active particle in a thermal environment. The stochasticity of the system entails that the particle behaves in an engine mode or refrigerator mode, when the respective protocols are applied, only in a suitably chosen range of parameters [3, 11]. We observe that although the engine mode for the active RT engine is generally less efficient than that of the passive engine (in contrast to the results of [4], where an active Brownian particle was used instead of an RT particle), the case is much more interesting when we compare the corresponding coefficients of performance in the refrigerator protocol. Using the refrigerator protocol, one can obtain a refrigerator whose performance is much better than the one using a passive particle as its working system.

In section 2, we describe the detailed model for the active engine, both in one and two dimensions. In section 3, we provide the numerical results for the efficiency of the active engines and their comparison with the corresponding passive ones. Section 4 discusses the results for the active particle subjected to the refrigerator protocol. Finally, the conclusions are provided in section 5.

## 2 The Model

An RT particle proceeds through a series of “runs” followed by “tumbles”, whose motion was first described in [22]. During the runs, the particle does not change direction and follows the path dictated by deterministic dynamics. However, at the end of a single run, the particle suddenly changes its direction randomly, and then sets into motion for another run along this newly chosen direction. The particle is thus said to tumble and choose a new direction in-between two run-times. Since the tumble times are typically an order of magnitude smaller than the typical run-times [24], we will approximate it to zero in our analysis. A typical trajectory of such a particle is shown in figure 1, in the space of normalized position coordinates (see the discussion below Eq. (8)). They symbols appear after every time step of integration. The persistence in motion over each runtime can be clearly observed.

The run times and tumble times have been shown to roughly follow exponential distributions [22, 32]. We therefore sample our run-times from the distribution

$$P(\tau_r) = \frac{1}{\tau_p} e^{-t/\tau_p}. \quad (1)$$

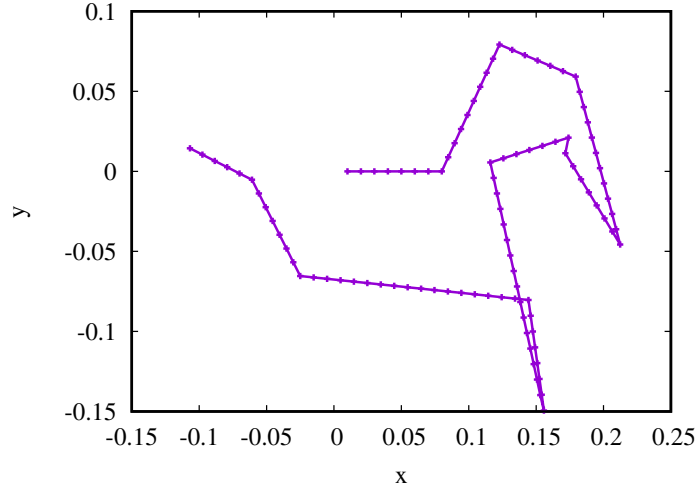


Figure 1: A typical trajectory of a 2d RT particle. The symbols represent individual time steps.

where  $\tau_p \equiv \langle \tau_r \rangle$  is the average run-time, which we refer to as the persistence time. Larger the persistence time is, more is the activity of the particle.

An exact mathematical description is lacking, although the asymptotic behaviour (in the limit of large time) can be shown to reach the diffusive regime [31]. We compare two different tumbling characteristics:

1. The particle undergoes complete reorientation (it can choose all possible deflection angles with equal probability).
2. The particle undergoes partial reorientation, where the probabilities of larger deflections are smaller. In particular, we choose the cosine distribution (see Eq. (6) below).

Our dynamics consists of the RT motion of the particle, as well as the thermal motion generated due the finite temperature of the medium in which the particle is present.

We consider the one dimensional model first, and then move on to study the two-dimensional model of the engine.

## 2.1 1d model

The particle experiences a potential  $V(x) = k(t)x^2/2$  created by an optical trap. In the case of total reorientation, it runs for a time  $\tau_r$  that is sampled from an exponential distribution given by Eq. (1).

The harmonic trap undergoes four steps corresponding to a Stirling cycle [4,6], given by:

1. **Step 1 (isothermal expansion):** the temperature is fixed at the higher value  $T_h$ , and  $k(t)$  varies linearly from the initial stiffness value  $k_0$  to the final value  $k_0/2$ , as per the following function of time:

$$k(t) = k_{\text{exp}}(t) = k_0 \left(1 - \frac{t}{\tau}\right), \quad 0 < t \leq \tau/2 \quad (2)$$

In this step, the particle is kept inactive for convenience. However, the dynamics still retains some randomness due the presence of the thermal noise of strength  $D_h = 2\gamma k_B T_h$ , where  $\gamma$  is the friction coefficient of the medium, and  $k_B$  is the Boltzmann constant.

2. **Step 2 (isochoric temperature increase):** The value of stiffness parameter is held constant, and the temperature is suddenly changed to the lower value  $T_c$ .

3. **Step 3 (isothermal compression):** The temperature is held constant at  $T_c$ , while the stiffness parameter changes from  $k_0/2$  to  $k_0$  as per the following linear function:

$$k(t) = k_{\text{com}}(t) = k_0 \left( \frac{t}{\tau} \right), \quad \tau/2 < t \leq \tau. \quad (3)$$

The activity of the particle is switched on at the beginning of this step. In this step, in addition to activity, a thermal noise of strength  $D_c = 2\gamma k_B T_c$  is present due to the finite temperature of the medium.

4. **Step 4 (isochoric temperature decrease):** In the final step, the temperature is suddenly increased to  $T_h$ , keeping the stiffness parameter fixed, so as to allow the engine to complete a cycle.

The functional form of  $k(t)$  is shown in figure 2.

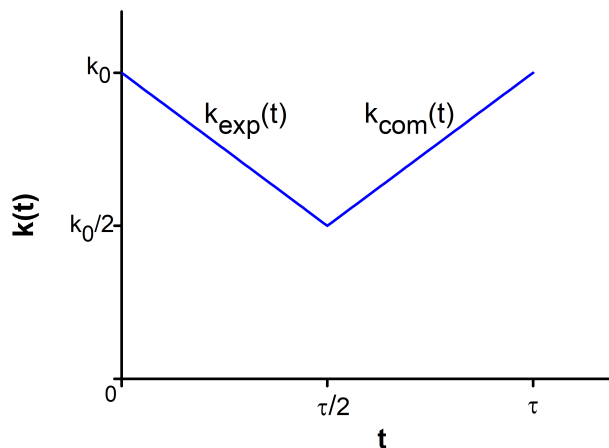


Figure 2: Variation of stiffness constant with time.

In the case of total reorientation, the particle moves either along the  $+x$  or  $-x$  direction for a time duration  $\tau_r$ , and then suddenly changes direction ( $+x \rightarrow -x$  or vice versa) with probability  $1/2$ . The persistence time is chosen to be much smaller than the cycle time, so that each isothermal step consists of several run-and-tumble events.

When the particle undergoes partial reorientation, it switches direction more reluctantly, with a probability  $p < 1/2$ . During the expansion step, the equation of motion of the particle is given by (see [23])

$$m\dot{v} = -\gamma v - k_e(t)x + (\sqrt{D_h})\xi(t), \quad 0 < t \leq \tau/2, \quad (4)$$

where  $\xi(t)$  is a normally distributed white noise:  $\langle \xi(t) \rangle = 0$ ,  $\langle \xi(t)\xi(t') \rangle = \delta(t - t')$ . During the compression step, the equation of motion *during the  $i^{\text{th}}$  run-time* is given by

$$m\dot{v}_i = -\gamma v_i - k_c(t)x + F + (\sqrt{D_c})\xi(t), \quad t_i < t \leq t_i + \tau_{r,i}. \quad (5)$$

Here,  $t_i$  is the initial time for the  $i^{\text{th}}$  run, which ends at time  $t_i + \tau_{r,i}$ . The active force  $F$  propels the particle in the chosen direction during a run [23]. In comparison to the expansion step, an added randomness is generated due to the possibility of a switch in the direction of velocity at the end of each run-time.

## 2.2 2d model

In this case, the particle is trapped in a 2d harmonic potential,  $V(x, y) = k(t)(x^2 + y^2)/2$ . We can describe the position vector of the particle by  $\mathbf{r} = x\hat{x} + y\hat{y}$  during a run-time ( $\hat{x}$  and  $\hat{y}$  are the unit vectors in the  $x$  and  $y$  directions, respectively), which changes to  $\mathbf{r}' = x'\hat{x} + y'\hat{y}$ , and the angle  $\theta$  between  $\mathbf{r}$  and  $\mathbf{r}'$  is the deflection attained due to the sudden tumble at the end of a run-time.

For the simple case of total reorientation, we use a uniform random number  $\eta$  at each tumble in the range  $\eta \in [-\pi, \pi]$ , and allow the value of the angle (with the  $x$ -axis, for convenience)  $\theta$  to change to  $\theta + \eta$ .

For the case of partial reorientation, we choose the distribution of the deflection to be of the form

$$P(\eta) = \frac{1}{4} \cos\left(\frac{\eta}{2}\right), \quad (6)$$

where the range is  $\eta \in [-\pi, \pi]$ . The method of obtaining the distribution has been given in appendix A.

The stiffness parameter  $k(t)$  undergoes the same set of steps as mentioned in section 2.1.

Let the total velocity be given by  $\mathbf{v} = v_x\hat{x} + v_y\hat{y}$ . Then the equations of motion are given by

$$\begin{aligned} m\dot{v}_x &= -\gamma v_x - k_e(t)x + (\sqrt{D_h})\xi(t), & 0 < t \leq \tau/2; \\ m\dot{v}_{x,i} &= -\gamma v_{x,i} - k_c(t)x + F_x + (\sqrt{D_c})\xi(t), & t_i < t \leq t_i + \tau_{r,i}, \end{aligned} \quad (7)$$

where  $\tau_{r,i}$  is the  $i^{\text{th}}$  run-time.  $\mathbf{F}$  is a self-propelling force that is directed along the axis of the particle, having components  $F_x = F \cos \theta$  and  $F_y = F \sin \theta$ . Similar equations can be written for motion in the  $y$ -direction.

## 3 Results and Discussions for stochastic engine using RT particle

### 3.1 Comparison with theory

We first test the outcomes of our simulation against theory. It was shown in [31] that the mean squared displacement of a two-dimensional RT particle (in the absence of any thermal bath or any potential) leads to the relations

$$\begin{aligned} \langle r^2 \rangle_{\text{tot}} &= 2v_0^2\tau_p^2 \left( \frac{t}{\tau_p} + e^{-t/\tau_p} - 1 \right); \\ \langle r^2 \rangle_{\text{par}} &= \frac{2v_0^2\tau_p^2}{1 - \sigma_1} \left[ \frac{t}{\tau_p} + \frac{e^{-(1-\sigma_1)t/\tau_p} - 1}{1 - \sigma_1} \right]. \end{aligned} \quad (8)$$

Here,  $\sigma_1 = \langle \cos(\eta) \rangle$  is the Fourier transform of the tumbling kernel (see [31]). The parameter  $v_0$  is the constant magnitude of the total velocity. On the other hand, in presence of thermal noise, the change in steady-state variance of an RT particle (without any potential) can be obtained using the approach of [23]. If the friction coefficient of the thermal bath is  $\gamma$  and its thermal noise strength is  $D$ , while the self-propelling force  $F$  is set to zero for analytical convenience, then the expression is given by (see appendix B for details)

$$\langle r^2(t) \rangle = \left[ \frac{2D\tau_p}{\gamma(m + \gamma\tau_p)} \right] t + \left[ \frac{2Dm\tau_p^2}{\gamma(m + \gamma\tau_p)^2} \right] \exp \left\{ -\frac{(m + \gamma\tau_p)t}{m\tau_p} \right\} - \frac{2Dm\tau_p^2}{\gamma(m + \gamma\tau_p)^2}. \quad (9)$$

We have shown these results in figure 3, where the simulation results have been obtained by using the Heun's method of integration (see [33]) over  $\sim 10^5$  realizations. In the figures, all times

are normalized by the cycle time  $\tau$ . All positions are normalized by the factor  $\sqrt{D_c\tau}$  ( $D_h$  and  $D_c$  are the diffusion constants for the hot and the cold reservoirs, respectively). This leads to a characteristic mass scale of  $\gamma\tau$  and characteristic force scale of  $\gamma\sqrt{D_c/\tau}$ . In figure 3(a), equations (8) have been compared with the results of simulations for total and partial reorientations. The symbols represent results of simulations, while the solid lines are the analytical results. Figure 3(b) compares Eq. (9) with simulation outcomes. In all the cases, the results of simulation are in good agreement with theoretical results. Unfortunately, the analytical treatments become intractable when the stiffness parameter becomes time-dependent, even in the overdamped limit.

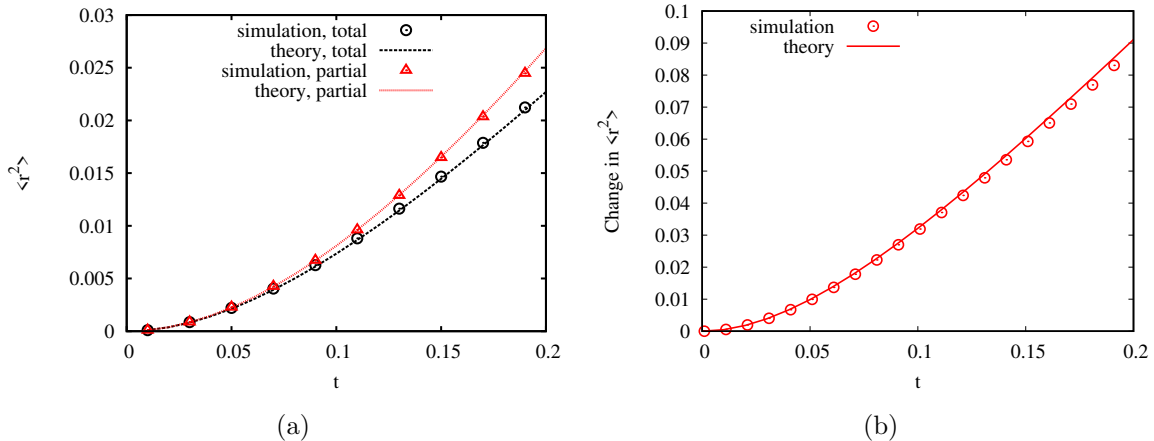


Figure 3: (a) Plots of the analytical solution in comparison to the numerical results for total reorientation (black solid line and black open circles, respectively) and for partial reorientation (red solid line and red open triangles respectively) of a 2d RT particle. The parameters are:  $m = 0.2$ ,  $\tau_p = 0.1$ . (b) Plots for the change in variance of the particle as a function of time in the steady state when thermal noise is present. The parameters are  $m = 0.2$ ,  $\tau_p = 0.1$ ,  $D = 1$ .

Intuitively, we would expect a partial reorientation to correspond to a higher activity as compared to total reorientation, since the former imparts a stronger persistence in the motion of the particle. In order to verify this, we have plotted the velocity correlations along  $x$ -direction  $\langle v_x(0)v_x(t) \rangle$  obtained for a particular set of parameters (as mentioned in the figure caption) in figure 4 as a function of time  $t$ . Figure 4(a) compares the velocity correlations for 1d and 2d RT particles, both for total and partial reorientations. As expected, the correlations are higher for partial reorientation in each case. Figure 4(b) compares the partial velocity correlations of the 1d and 2d particles with those of the corresponding passive particles. We find that the correlations are in general weaker for the RT particles, due to the degradation in the correlations caused by tumble events.

### 3.2 Efficiency of the 1d active RT engine

We now proceed with the calculation of efficiency of an engine using a 1d active particle by simulating the dynamics of the engine (see Eqs. (4) and (5)). The work done on the particle is calculated by using the definition prescribed by Stochastic Thermodynamics [34, 35]:

$$W(t) = \frac{1}{2} \int_0^t \dot{k}(t') x^2(t') dt'. \quad (10)$$

The average work extracted can be calculated from the variance, defined as  $\sigma(t) = \langle x^2(t) \rangle$ , by means of the relation

$$\langle W(t) \rangle = \frac{1}{2} \int_0^t \dot{k}(t') \sigma(t') dt'. \quad (11)$$

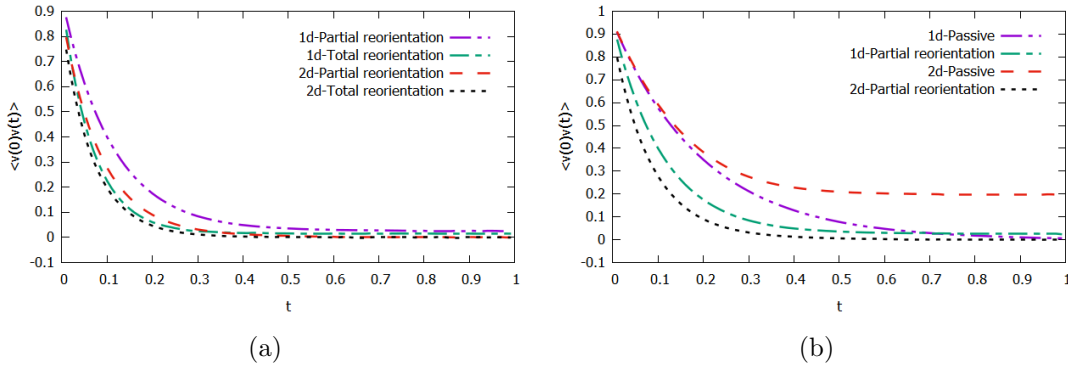


Figure 4: (a) Velocity correlations  $\langle v_x(0)v_x(t) \rangle$  as a function of time for a 1d and a 2d RT particle in the case of total and partial reorientations. The parameters used are  $m = 0.2$ ,  $\tau_p = 0.1$ ,  $F = 0.1$ ,  $D = 0.01$ ,  $k_0 = 0$ . (b) Velocity correlations for 1d and 2d passive and active particle with partial reorientation. Parameters used are same as in (a).

The average heat absorbed in the expansion step is given by the first law:

$$\langle Q \rangle_h = \langle W \rangle_h - \langle \Delta E \rangle_h, \quad (12)$$

where the subscript  $h$  implies that only the expansion step (when system is in contact with hot reservoir) is considered. The sign convention is such that the work done *on* the system and the heat dissipated *by* the system are positive, which is why the extracted work and absorbed heat must be given by  $-\langle W \rangle$  and  $-\langle Q \rangle_h$ , respectively. The average change in internal energy  $\langle E \rangle$  during the expansion step is given by

$$\langle \Delta E \rangle_h = \frac{1}{2}k(\tau/2)\sigma(\tau/2) - \frac{1}{2}k(0)\sigma(0). \quad (13)$$

The efficiency is obtained using the standard relation

$$\eta = \frac{\langle W \rangle}{\langle Q \rangle_h} = \frac{\langle W \rangle}{\langle W \rangle_h - \langle \Delta E \rangle_h}. \quad (14)$$

We now compare the efficiencies of the active and passive engines, when the engine has settled into a time-periodic steady state, i.e. when the variance becomes periodic in time, (see figure 5 (a)). We observe that the efficiency of the passive engine is higher than the active engine with partial reorientation, the latter being in turn slightly higher than the active engine with total reorientation. In figure 5(b), we plot the variation in efficiency with the persistence time  $\tau_p$ . We find that the efficiency for the 1d active engine is almost independent of the persistence time. The plots clearly bring out the fact that the overdamped particle ( $m \ll \gamma$ ) is much more efficient as compared to the underdamped one. The reason is that, for a massive particle, the effect of the potential is much smaller, so that the variance keeps increasing even in the compression step. This leads to a large amount of work being pumped into the system, thus reducing the net work extracted in the entire cycle.

### 3.3 Efficiency of a 2d RT engine

As mentioned above, for the partial reorientation of 2d RT particle, we choose the tumble angles from the distribution  $P(\eta) = \cos(\eta/2)/4$ . The details for generating this distribution numerically has been provided in appendix A. In figure 6(a), we plot the efficiencies as a function of mass of the particle, for the passive engine and active engines (with partial and total reorientations respectively). We find that the qualitative trends obtained for 1d engine (see figure 5) holds for the 2d engine as well, but the difference between efficiencies due to partial and total

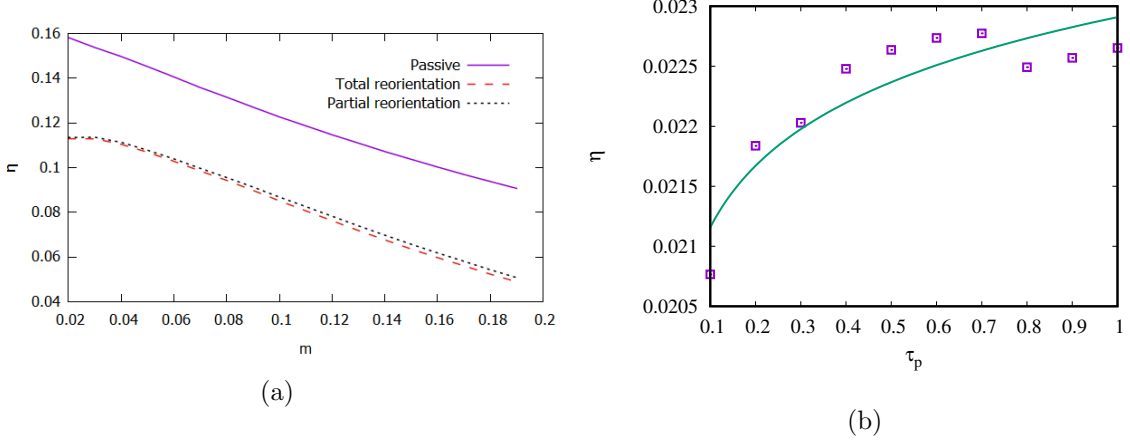


Figure 5: (a) Plot of efficiency with mass in 1d for the passive engine (purple solid line), active engine with total reorientation (red dashed line) and with partial reorientation (black dotted line). The parameters are  $D_c = 1$ ,  $k_0 = 50$ ,  $\tau_p = 0.2$ ,  $F = 0.1$ . (b) Plot showing variation of efficiency as a function of the persistence time. The symbols show results of simulation, while the solid line is the best fit ( $\sim \tau_p^{0.035}$ ).

reorientations is negligible. Figure 6(b) shows the variation of efficiency of the 2d active engine with the persistence time  $\tau_p$ . We find that the efficiency shows a slow decrease with the increase in  $\tau_p$ .

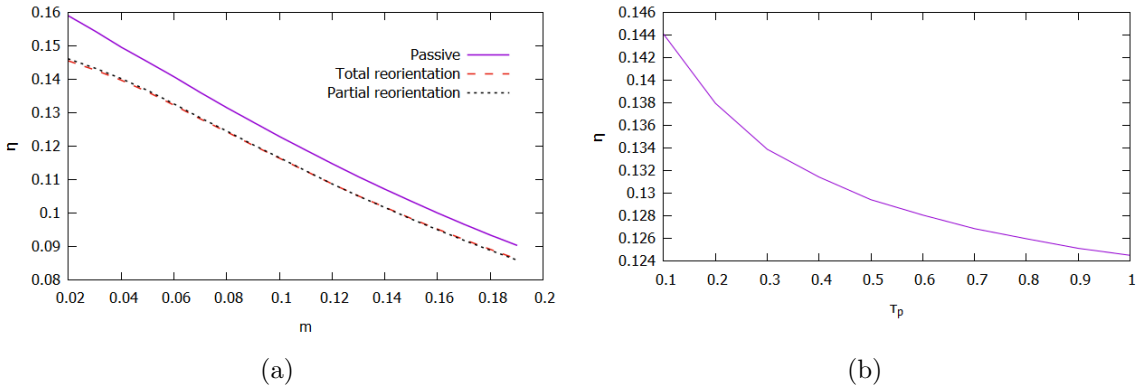


Figure 6: (a) Plot of efficiency with mass in 2d for the passive engine (purple solid line), active engine with total reorientation (red dashed line) and with partial reorientation (black dotted line). Parameters used are:  $D_c = 1$ ,  $D_h = 2$ ,  $k_0 = 50$ ,  $\tau_p = 0.2$ ,  $F = 0.1$ . (b) Plot showing variation of efficiency as a function of the persistence time.

## 4 RT particle used as a refrigerator

In this section, we study the behaviour of the RT particle undergoing partial reorientations in one and two dimensions, by reversing the engine protocol, as shown in figure 7.

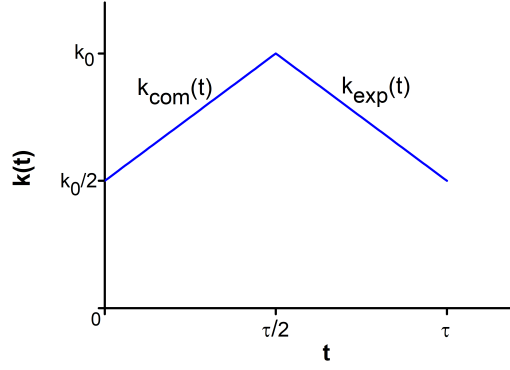


Figure 7: Variation of stiffness parameter for refrigerator mode.

The time-dependences are given by

$$\begin{aligned} k_{\text{com}}(t) &= k_0 \left( \frac{1}{2} + \frac{t}{\tau} \right), & 0 < t \leq \tau/2; \\ k_{\text{exp}}(t) &= k_0 \left( \frac{3}{2} - \frac{t}{\tau} \right) & \tau/2 < t \leq \tau. \end{aligned} \quad (15)$$

The sequence of steps are:

1. **Isothermal compression** at temperature  $T_h$ , changing stiffness constant from  $k_0/2$  to  $k_0$ .
2. **Isochoric decrease of temperature** from  $T_h$  to  $T_c$ . The stiffness parameter remains fixed at  $k_0$ .
3. **Isothermal expansion** at temperature  $T_c$ , changing the stiffness constant from  $k_0$  to  $k_0/2$ .
4. **Isochoric increase of temperature** from  $T_c$  to  $T_h$ . The stiffness parameter remains fixed at  $k_0/2$ .

The *coefficient of performance* (COP) of a refrigerator is defined as the ratio of the heat removed from the cold reservoir to the work done in the full cycle:

$$\text{COP} = -\frac{\langle Q \rangle_c}{\langle W \rangle} = -\frac{\langle W \rangle_c - \langle \Delta E \rangle_c}{\langle W \rangle}. \quad (16)$$

The subscript  $c$  refers to the fact that the quantities have been computed when the particle is in contact with the cold reservoir.

For a reversible engine, we find that

$$\text{COP} = \frac{T_c}{T_h - T_c} = \frac{T_c}{\eta_{\text{rev}} T_h} \quad (17)$$

where  $\eta_{\text{rev}} \equiv (1 - T_c/T_h)$  is the Carnot efficiency in the engine mode. Thus, in the nonequilibrium regime, it would be reasonable to expect that a more efficient engine when run in reverse would give a refrigerator with smaller COP, and vice versa. Keeping this in mind, we study the thermodynamics of the active refrigerator and check whether it can have a higher value of COP than a passive refrigerator in a suitable range of parameters.

In figure 8(a) and 8(b) respectively, we plot the variation of the COP with the mass for 1d and 2d active (partial reorientation) and passive particles. For a suitable range of parameters

(see figure caption), the active refrigerator is observed to have a higher COP than the passive one. In fact, the former continues to act as a refrigerator ( $\langle Q \rangle_c < 0$ ,  $\langle W \rangle > 0$ ) even for higher masses where the passive particle ceases to be in the refrigerator mode.

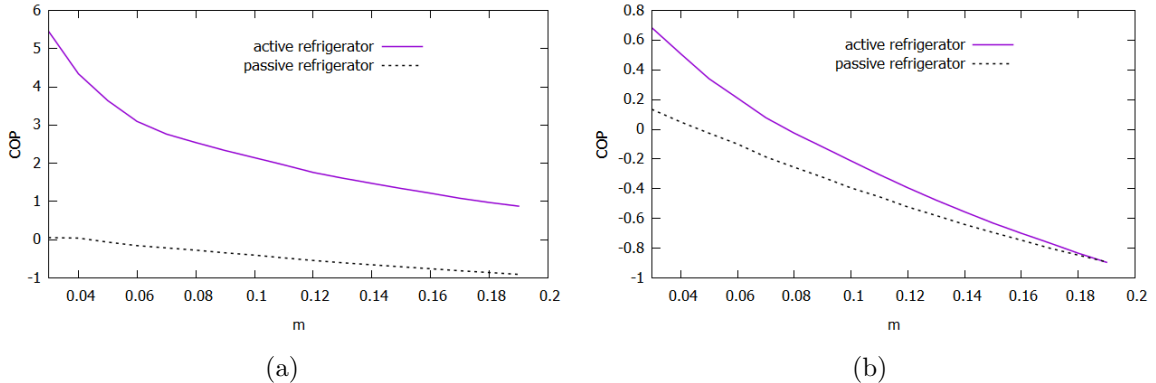


Figure 8: (a) Plot of the coefficient of performance of the 1d refrigerator with partial reorientation as a function of the mass of the particle. The parameters are:  $F = 0.1$  (for active particle),  $D_h = 1.25$ ,  $D_c = 1$ ,  $\tau_p = 0.2$ .(b) Similar plot for 2d refrigerator.

In figure 9, we show the phase plot indicating the variation of the COP of the refrigerators as a function of the thermal noise  $D_h$  of the hot bath and of the mass  $m$  of the particle. One can easily observe the higher value of COP at smaller mass, in particular near the bottom left corner of the plots. Moreover, it can further be noted that the active refrigerators clearly outperform the passive ones (in terms of the magnitudes of COP) in this range of parameters (see caption). One also observes that as the noise strength  $D_h$  of the hot thermal bath is increased (i.e.  $T_h$  is increased) with the other parameters held fixed, the value of COP decreases. This is expected on the grounds that with an increased difference between the temperatures of the two baths, the thermal drive makes a stronger attempt to drive the flow of energy in the opposite direction. One can further observe that the system acts as a refrigerator in a larger range of parameters for the passive particle, whereas for the active refrigerator this region gets shifted towards further left in the figure. In particular for the active system, the refrigerator mode is available for the 2d system in a smaller range of parameters than in the case of the 1d system. Overall, we find that although the engine using RT particle as its working substance finds it hard to beat the performance of a passive engine, the situation is quite different when one deals with the corresponding refrigerators by time-reversing the protocols.

We now study the dependence of COP on the persistence time  $\tau_p$  in figure 10. The COP for 1d and 2d refrigerators with partial reorientations are shown in figures 10 (a) and (b), respectively, in the limit of small mass (overdamped particle). Clearly, the 1d refrigerator has higher values of COP than the 2d one, in the chosen parameter range. Interestingly, the COP for 1d RT refrigerator decreases with increase in  $\tau_p$ , whereas the trend is opposite for the 2d RT refrigerator. Nevertheless, they are always appreciably higher than the COP for the corresponding passive refrigerator, for which the values of COP are 0.67 and 0.72 in 1d and 2d respectively (for the set of parameters mentioned in the figure caption).

Figure 11 shows the phase plot for COP as a function of  $\tau_p$  and  $D_h$ . We notice that although the 1d active system works in the refrigerator mode within a smaller range of parameters, the values of COP are much larger than the 2d refrigerator. The decrease of COP with increase in  $D_h$  is expected, as per the discussion on figure 9. We notice that the variation in COP with  $\tau_p$  is quite small, although the 2d refrigerator shows a clear increase in COP with increase in  $\tau_p$  around  $D_h = 1.2$ , which was observed in figure 10.

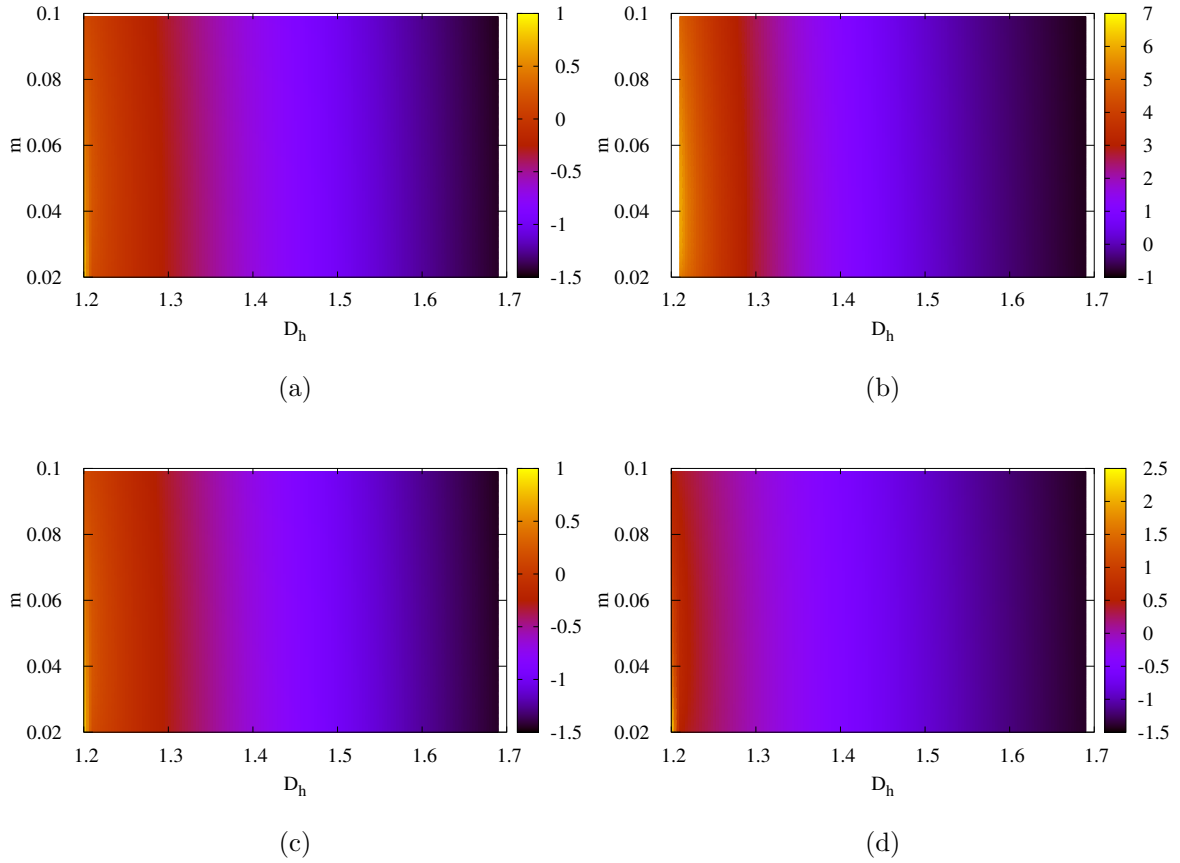


Figure 9: Phase plot of COP as a function of  $D_h$  and  $m$  for (a) 1d passive refrigerator, (b) 1d active refrigerator, (c) 2d passive refrigerator and (d) 2d active refrigerator. Parameters are  $D_c = 1$ ,  $k_0 = 50$ ,  $\tau_p = 0.2$ .

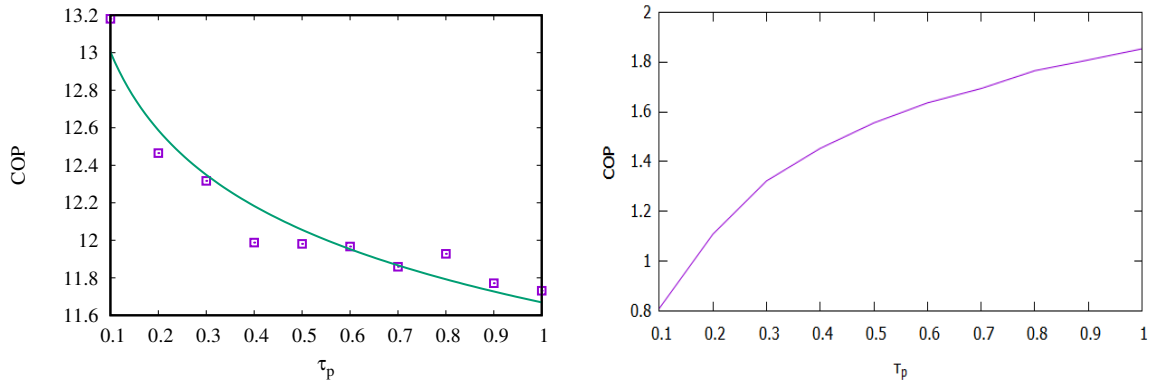


Figure 10: (a) Plot showing COP of a 1d refrigerator (with partial reorientation) as a function of  $\tau_p$ . The symbols represent results of simulation and the solid line is the best fit ( $\sim \tau_p^{-0.047}$ ). The parameters used are:  $k_0 = 50$ ,  $D_c = 1$ ,  $D_h = 1.2$ ,  $F = 0.1$ ,  $m = 0.03$ . (b) Similar plot for a 2d refrigerator.

## 5 Conclusions

Microscopic thermal machines have been studied extensively in recent years. Modelling of such machines using a trapped particle in a confining potential has been studied. Recent works

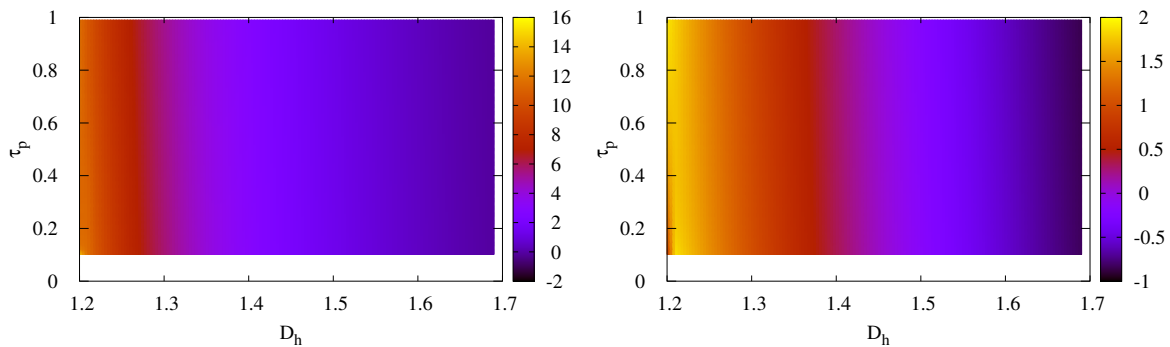


Figure 11: (a) Phase plot of COP as a function of  $\tau_p$  and  $D_h$  for the 1d active refrigerator. (b) Similar plot for 2d active refrigerator. Parameters used in the plots are:  $D_c = 1$ ,  $m = 0.03$ ,  $F = 0.1$ ,  $k_0 = 50$ .

show that if a heat engine at such small scales use an active Brownian particle as its working system, it can lead to a higher efficiency than that using a passive Brownian particle. We study a microscopic Stirling engine using an active particle, but the activity is introduced by run-and-tumble motion of the particle. In this case, when the engine protocol is used and the system works in the engine mode (heat is absorbed on average from the hot bath and work is extracted in the cycle), we find that the efficiency is less than that of a passive engine. However, if we apply the reservoir protocol by time-reversing the engine protocol, in a suitably chosen parameter regime, the active refrigerator can give rise to a far higher coefficient of performance as compared to its passive counterpart. Both efficiency (for the engine) and COP (for the refrigerator) are higher when the particle mass becomes smaller. An RT motion that involves partial reorientations at the tumble events gives only a minor improvement over that involving total reorientations. It would be interesting to see how far the above conclusions hold for quantum thermal engines, where RT motions may be imposed by means of external fields.

## 6 Acknowledgments

The authors thank DST-SERB (grant number ECR/2017/002607) for funding. SL thanks S. Chaki for suggesting useful references.

## References

- [1] Yamaan Saadeh and Dinesh Vyas. Nanorobotic applications in medicine: Current proposals and designs. *Am. J. Robotic Surgery*, 1:4, 2014.
- [2] T. Schmeidl and U. Seifert. Efficiency at maximum power: An analytically solvable model for stochastic heat engines. *Europhys. Lett.*, 81:20003, 2008.
- [3] Arnab Saha and Rahul Marathe. Stochastic work extraction in a colloidal heat engine in the presence of colored noise. *J. Stat. Mech: Theor. Exp*, page 094012, 2019.
- [4] Aradhana Kumari, P. S. Pal, Arnab Saha, and Sourabh Lahiri. Stochastic heat engine using an active particle. *Phys. Rev. E*, 101:032109, 2020.
- [5] I. A. Martinez, E. Roldan, L. Dinis, D. Petrov, J. M. R. Parrondo, and R. A. Rica. Brownian carnot engine. *Nat. Phys.*, 12:67, 2016.

- [6] Valentin Blickle and Clemens Bechinger. Realization of a micrometre-sized stochastic heat engine. *Nature Physics*, 8:143, 2012.
- [7] Johannes Roßnagel, Samuel T. Dawkins, Karl N. Tolazzi, Obinna Abah, Eric Lutz, Ferdinand Schmidt-Kaler, and Kilian Singer<sup>1</sup>. A single-atom heat engine. *Science*, 352:325, 2016.
- [8] Ignacio A. Martínez, Édgar Roldán, Luis Dinis, and Raúl A. Rica. Colloidal heat engines: a review. *Soft Matter*, 13:22, 2017.
- [9] Carl M Bender, Dorje C Brody, and Bernhard K Meister. Quantum mechanical carnot engine. *J. Phys. A*, 33:4427, 2000.
- [10] H. T. Quan, Yu xi Liu, C. P. Sun, and Franco Nori. Quantum thermodynamic cycles and quantum heat engines. *Phys. Rev. E*, 76:031105, 2007.
- [11] Shubhashis Rana, P.S. Pal, Arnab Saha, and A.M. Jayannavar. Anomalous brownian refrigerator. *Physica A*, 444:783, 2016.
- [12] P. S. Pal, Arnab Saha, and A. M. Jayannavar. Operational characteristics of single-particle heat engines and refrigerators with time-asymmetric protocol. *International Journal of Modern Physics B*, 30:1650219, 2016.
- [13] Bao-Quan Ai, Liqiu Wang, and Liang-Gang Liu. Brownian micro-engines and refrigerators in a spatially periodic temperature field: Heat flow and performances. *Phys. Lett. A*, 352:286, 2006.
- [14] Bihong Lin and Jincan Chen. Performance characteristics and parametric optimum criteria of a brownian micro-refrigerator in a spatially periodic temperature field. *J. Phys. A: Math. Theor.*, 42:075006, 2009.
- [15] Lingen Chen, Zemin Ding, and Fengrui Sun. A generalized model of an irreversible thermal brownian refrigerator and its performance. *Applied Mathematical Modelling*, 35:2945, 2010.
- [16] Shoudan Liang, David Medich, Daniel M. Czaikowsky, Sitong Sheng, Jian-Yang Yuan, and Zhifeng Shao. Thermal noise reduction of mechanical oscillators by actively controlled external dissipative forces. *Ultramicroscopy*, 84:119, 2000.
- [17] Kyung Hyuk Kim and Hong Qian. Entropy production of brownian macromolecules with inertia. *Phys. Rev. Lett.*, 93:120602, 2004.
- [18] Kyung Hyuk Kim and Hong Qian. Fluctuation theorems for a molecular refrigerator. *Phys. Rev. E*, 75:022102, 2007.
- [19] Hans J. Briegel and Sandu Popescu. Entanglement and intra-molecular cooling in biological systems? - a quantum thermodynamic perspective, 2008.
- [20] Noah Linden, Sandu Popescu, and Paul Skrzypczyk. How small can thermal machines be? the smallest possible refrigerator. *Phys. Rev. Lett.*, 105:130401, 2010.
- [21] Nicolas Brunner, Marcus Huber, Noah Linden, Sandu Popescu, Ralph Silva, , and Paul Skrzypczyk. Entanglement enhances cooling in microscopic quantum refrigerators. *Phys. Rev. Lett.*, 89:032115, 2014.
- [22] Howard C. Berg and Douglas A. Brown. Chemotaxis in escherichia coli analyzed by three-dimensional tracking. *Nature*, 239:500, 1972.

- [23] C. A. Condat, J. Jäckle, and S. A. Menchón. Randomly curved runs interrupted by tumbling: A model for bacterial motion. *Phys. Rev. E*, 72:021909.
- [24] G. Fier, D. Hansmann, and R. C. Buceta. A stochastic model for directional changes of swimming bacteria. *Soft Matter*, 13:3385, 2017.
- [25] G. Fier, D. Hansmann, and R. C. Buceta. Langevin equations for the run-and-tumble of swimming bacteria. *arxiv/cond-mat:1802.00269*, 2018.
- [26] Mark J. Schnitzer. Theory of continuum random walks and application to chemotaxis. *Phys. Rev. E*, 48:2553, 1993.
- [27] Abhishek Dhar, Anupam Kundu, Satya N. Majumdar, Sanjib Sabhapandit, and Grégory Schehr. Run-and-tumble particle in one-dimensional confining potentials: Steady-state, relaxation, and first-passage properties. *Phys. Rev. E*, 99:032132, 2019.
- [28] M. E. Cates and J. Tailleur. When are active brownian particles and run-and-tumble particles equivalent? consequences for motility-induced phase separation. *Europhys. Lett.*, 101:20010, 2013.
- [29] J. Elgeti, R. G. Winkler, and G. Gompper. Physics of microswimmers: single particle motion and collective behavior: a review. *Rep. Prog. Phys.*, 78:056601, 2015.
- [30] Tomoyuki Manoa, Jean-Baptiste Delfauc, Junichiro Iwasawaa, and Masaki Sano. Optimal run-and-tumblebased transportation of a janus particle with active steering. *PNAS*, 114:E2580–E2589, 2017.
- [31] Andrea Villa-Torrealba, Cristóbal Chávez-Raby, Pablo de Castro, , and Rodrigo Soto. Run-and-tumble bacteria slowly approaching the diffusive regime. *Phys. Rev. E*, 101:062607, 2020.
- [32] Douglas A. Brown and Howard C. Berg. Temporal stimulation of chemotaxis in escherichia coli. *Proc. Nat. Acad. Sci. USA*, 71:1388, 1974.
- [33] R. Manna. *Stochastic process in physics, chemistry and biology*. J. A. Freun and T. Pöschel eds., Springer-Verlag, Berlin, , 2000.
- [34] K. Sekimoto. Kinetic characterization of heat bath and the energetics of thermal ratchet models. *Prog. Theor. Phys. Supp.*, 130:17, 1998.
- [35] Ken Sekimoto. *Stochastic Energetics*. Springer, 2010.
- [36] Luc Devroye. *Non-Uniform Random Variate Generation*. Springer New York, 1986.

## A Cosine distribution

To generate the distribution, we have used the technique of inverse transform sampling (ITS) [36]. The cumulative density function (CDF) for  $P(\eta)$  is given by

$$F(\eta) = \frac{1}{4} \int_{-\pi}^{\eta} \cos\left(\frac{\eta'}{2}\right) d\eta' = \frac{1}{2} \left[1 + \sin\left(\frac{\eta}{2}\right)\right]. \quad (18)$$

Its inverse is given by

$$\eta = 2 \sin^{-1}[2F(\eta) - 1]. \quad (19)$$

Following the method of ITS, we define the random variable in the  $i^{\text{th}}$  iteration to be

$$\eta_i = 2 \sin^{-1}(2u_i - 1), \quad (20)$$

where  $u_i$  is a uniform random number in the range  $[0,1]$ . The figure 12 shows that the distribution of  $\eta_i$  indeed follows the desired form.

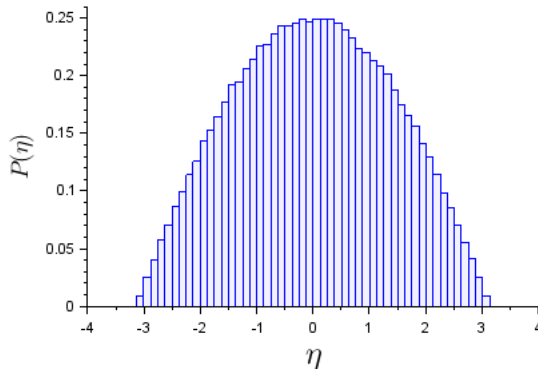


Figure 12: Distribution of tumble angle  $\eta$ .

## B Variance of RT particle in presence of thermal noise

Consider the equation

$$m\dot{v} = -\gamma v + (\sqrt{D})\xi(t). \quad (21)$$

which is interrupted by tumbles. In absence of tumble events, the velocity correlation is given by

$$\langle v_x(t_1)v_x(t_2) \rangle = \langle v_y(t_1)v_y(t_2) \rangle = \frac{D}{2m\gamma} e^{-\gamma|t_1-t_2|/m}; \quad (22)$$

The variance in absence of tumble events is therefore given by

$$\langle x^2(t) \rangle = \int_0^t dt_1 \int_0^t dt_2 \langle v_x(t_1)v_x(t_2) \rangle = \langle y^2(t) \rangle. \quad (23)$$

The variance in absence of tumble events is given by

$$\sigma(t) \equiv \langle x^2(t) \rangle + \langle y^2(t) \rangle = \frac{2D}{\gamma^2} t - \frac{2Dm}{\gamma^3} \left(1 - e^{-\gamma t/m}\right). \quad (24)$$

Next, let us include tumble events. If the probability of a run duration  $\tau_r$  is given by  $P(\tau_r)$ , then the probability that no tumble has taken place in time  $t$  is given by

$$Q(t) = 1 - \int_0^t P(t') dt', \quad (25)$$

so that the modified variance in the presence of tumble events is

$$\langle r^2(t) \rangle = Q(t)\sigma(t) + \int_0^t P(t')[\sigma(t') + \sigma(t-t')] dt'. \quad (26)$$

The first term on the RHS is the contribution from uninterrupted runs, the second term is that of first run and the third is due to subsequent runs. If we define the function

$$f(t) = Q(t)\sigma(t) + \int_0^t P(t')\sigma(t') dt', \quad (27)$$

then performing Laplace transform on both sides, we get

$$\tilde{\sigma}(s) = \frac{\tilde{f}(s)}{1 - \tilde{P}(s)}. \quad (28)$$

Finally, performing the inverse Laplace transform, we obtain eq. (9).